THE JOURNAL OF PHYSICAL CHEMISTRY B

Article

pubs.acs.org/JPCB

# Simulations of Tryptophan Fluorescence Dynamics during Folding of the Villin Headpiece

Jose R. Tusell and Patrik R. Callis*

Department of Chemistry and Biochemistry, Montana State University, Bozeman, Montana 59717-3400, United States

Supporting Information

**ABSTRACT:** Protein folding kinetics is commonly monitored by changes in tryptophan (Trp) fluorescence intensity. Considerable recent discussion has centered on whether the fluorescence of the single Trp in the much-studied, fast-folding villin headpiece C-terminal domain (HP35) accurately reflects folding kinetics, given the general view that quenching is by a histidine cation ($His^+$) one turn away in an $\alpha$-helix (helix III) that forms early in the folding process, according to published MD simulations. To help answer this question, we ran 1.0 $\mu$s MD simulations on HP35 (N27H) and a faster-folding variant in its folded form at 300 K and used the coordinates and force field charges with quantum calculations to simulate fluorescence quenching caused by electron transfer to the local amide and to the $His^+$. The simulations demonstrate that quenching by $His^+$ in the fully formed helix III is possible only during certain Trp and $His^+$ rotamer and solvent conformations, the propensity of which is a variable that can allow Trp fluorescence to report the global folding rate, as recent experiments imply.

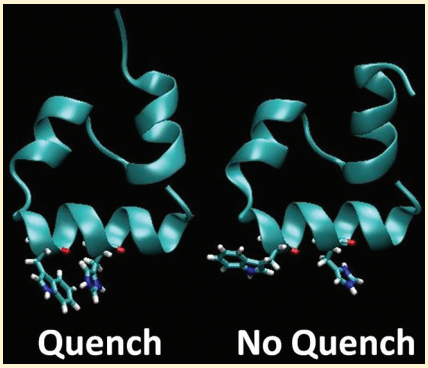


## INTRODUCTION

The high sensitivity of the amino acid tryptophan (Trp) fluorescence wavelength, intensity (quantum yield), and lifetime in proteins is responsible for its wide use in following a myriad of protein processes.[1−3] Often, knowledge of the precise mechanism underlying the change in Trp fluorescence is not required to extract the rate and extent of the process of interest. In recent years, however, Trp fluorescence has been increasingly exploited to follow the rate of protein folding/unfolding.[4,5] Given the vast variety of local environments expected for a Trp during the process of folding and the fact that the quantum yield ($\Phi_f$) for single-Trp proteins varies from ~0.35 down to <0.01, one can legitimately wonder whether dynamic changes in fluorescence quantum yield are a faithful measure of folding dynamics. Indeed, the accuracy of fluorescence as an indicator of folding rate has been brought into question in the comparison of simulated and experimental folding rates for the C-terminal domain of the villin headpiece mutants HP35 N27H (PDB = 1YRF; hereafter called HP35) and HP35 N27H K24Nle K29Nle (PDB = 2F4K), wherein classical molecular dynamics (MD) simulations predict folding times that are several microseconds longer[6,7] than experiment.[5,8,9] These proteins are among a series designed by Eaton and co-workers to exploit the quenching of a single Trp by the strong collisional quencher $His^+$ through an i,i+4 interaction in a helix, both in HP35[5,8,10] and shorter helical peptides.[11−13] In villin, MD simulations suggest that the helix in question is formed much before the final folded structure is achieved.[6,7] On the other hand, recent reports support the ability of fluorescence to report the global folding rate. Cellmer et al. show that a Cys placed at the N-terminus, which quenches the triplet state of Trp23 in helix III in the unfolded state, gives the same fast folding rate as that deduced from Trp23 fluorescence.[9] Reiner et al.[14] find a similar folding rate from triplet−triplet energy-transfer experiments (TTET). Beauchamp et al.[15] show that the latter experiments are in accord with MD simulations. Simulations by Piana et al.[16] show that the accessible surface area (SASA) of Trp23 of the fast-folding mutant of villin HP35 N27H K24Nle K29Nle has the same autocorrelation time during 100 $\mu$s simulations at the melting temperature as the rmsd and the number of native side-chain contacts.

In an effort to understand how the seemingly local Trp−$His^+$ quenching can or cannot report the global folding rate, we combine MD simulations with quantum mechanics (MD + QM) with explicit solvent to make predictions of fluorescence lifetimes and quantum yields for villin. We have previously demonstrated that the extreme variability of the Trp fluorescence intensity in different protein environments stems generally from the large sensitivity to the local electric field of the energy of a charge-transfer (CT) state resulting from electron transfer (ET) from the excited indole ring to one of the two closest backbone amides.[17−23] When the electric potential at the weakly electron accepting amide is sufficiently positive relative to the ring, facile ET resulting in fluorescence quenching is enabled. The same principles apply to quenching by $His^+$. We will show in this paper that while amide quenching is strong in villin, it is insensitive to folding, and we focus

**Received:** November 21, 2011
**Revised:** January 17, 2012
**Published:** January 18, 2012





dx.doi.org/10.1021/jp211217w | J. Phys. Chem. B 2012, 116, 2586−2594

mainly on the quenching by $His^+$,[24−26] which apparently is essential to following folding.

This paper is divided into two sections. First, we demonstrate that by using a different MD program/force field and 1000-fold longer simulations than those in our previous studies, the predictive power of the method is much the same as that found previously. Second, we report three 1 $\mu$s MD + QM simulations for HP35, in which we apply our method to determine fluorescence quantum yields and lifetimes from rates of ET to the amide backbone and the histidine cation from calculations. The results reveal a heretofore unexpected heterogeneity in the fluorescence behavior of Trp in the fully formed helix. The impact of this heterogeneity on the modest change in quantum yield due to $His^+$ quenching during unfolding is discussed in terms of how such a seemingly local switching might reflect global folding.

## METHODS

**MD Simulations.** The 25 ns simulations were carried out for 20 single-Trp proteins starting from a crystal structure, using GROMACS 4.0.7 with the OPLS force field. Each protein was solvated to have at least 1 nm of TIP3P water from the surface of the protein. Chloride or sodium ions were added to neutralize the charge of the protein. An energy minimization was carried out until the maximum force on all atoms was less than 1000 kJ/mol·nm. *NVT* and *NPT* equilibrations were carried out for 100 ps each. The time step was 2 fs, and all covalent bonds were constrained by a force of 1000 kJ/mol·nm. Electrostatics were carried out using particle mesh Ewald. The pressure and temperature were set at 1.0 bar and 300 K. The temperature was controlled with a Berendsen thermostat with a 0.1 ps time constant. The pressure was controlled with a Parinello−Rahman barostat with a 2.0 ps time constant. Periodic boundary conditions were used with a cubic box as the unit cell. After equilibration, a 25 ns production simulation was carried out under *NPT* conditions, with the pressure and temperature set at 1.0 bar and 300 K, respectively. Coordinates were saved every 2 ps for a total of 12500 snapshots per simulation.

**Calculation of Quenching by Amide.** Estimating the quenching rate by ET to the local amides, as modified by the local electrostatic potential landscape, has been an ongoing project.[17,18,20−23] In general, we calculate fluorescence quantum yields using the formula

$$\Phi_f = \frac{k_r(\lambda)}{k_r(\lambda) + k_{nr}(\lambda) + k_{ET,Am} + k_{ET,His^+}} \quad (1)$$

where $k_r(\lambda)$ and $k_{nr}(\lambda)$ are the radiative rate and internal nonradiative first-order rate constants for Trp in the fluorescing state ($^1L_a$), respectively; $k_{ET,Am}$ and $k_{ET,His^+}$ are the rate constants for ET (quenching) from $^1L_a$ to the nearest backbone amide and to $His^+$ (if in close contact). The values for a given fluorescence maximum wavelength ($\lambda$) are extrapolated from study of the lifetime and quantum yield in different solvents by Meech et al.[27] In the present work, we use the values for 3-methylindole (3MI) in water at 298 K, $k_r = 4 \times 10^7$ $s^{-1}$ and $k_{nr} = 8 \times 10^7$ $s^{-1}$, giving $\Phi_f = 0.33$ for the unquenched Trp chromophore.[26] The ET rate constants, $k_{ET,Am}$ and $k_{ET,His^+}$, are therefore the primary determinants of the quantum yields. Different proteins will have different average $k_{ET}$ values due to the different average electrostatic environments. Important in the present work is that $k_{ET}$ may be a heterogeneous property of a given protein ensemble. $k_{ET}$ is calculated using Fermi's golden rule

$$k_{ET}(\Delta E_{00}) = \frac{2\pi}{\hbar}|V_{ET}^2|\rho_{FC}(\Delta E_{00}) \quad (2)$$

$V_{ET}$ is the Hamiltonian matrix element of the ET coupling the CT and fluorescing state ($^1L_a$), $\rho_{FC}$ is the Franck−Condon weighted density of final states (FCDOS), which is a function of $\Delta E_{00}$, and $\Delta E_{00}$ is the important energy gap between the zero-point levels of the CT and the fluorescing state ($^1L_a$). The variables in eq 2 were computed from the MD coordinate snapshots of all protein and solvent atoms. The vertical transition energy to the first 60 excited states of the Trp and its two covalently connected backbone amides (in the form of *N*-formyltryptophanamide) were calculated using Zerner's INDO/S-CIS,[28,29] in which potentials from the point charges of the protein and solvent representation in the MD force field are incorporated into the Hamiltonian. From the QM charge densities, the $^1L_a$ and amide CT states were identified. $\rho_{FC}(\Delta E_{00})$ comes from the overlap of Franck−Condon factor densities for ionization of the indole ring and electron attachment of the amide group, as described previously.[18,20,23] $\Delta E_{00}$ determines the magnitude of $\rho_{FC}$ and is determined by shifting the Zindo energy gap upward by a semiempirical constant, 240 $cm^{-1}$, based on a best fit to experimental quantum yields from the set of 20 Trps in 17 proteins used previously.[20] The value used here differs considerably from the value of 5000 $cm^{-1}$ used in the previous work because we chose for expediency to use ground-state geometry for the chromophore in the much faster GROMACS program, instead of CT state geometries in our previous CHARMM simulations.

$V_{ET}$ was calculated from CIS Hamiltonian matrix elements using Gaussian03, as described previously.[20] The read window was from the HOMO to LUMO+2 for amide quenching and from the HOMO to LUMO+4 for the 4-methylimidazole cation ($4MIm^+$)/3MI supermolecule. These matrix elements were computed in vacuum using the MD geometries and were corrected to account for extensive mixing of orbitals.

As in the previous work,[20] when the relaxation following a change in charge distribution to that of the CT state (reorganization energy) does not exceed the mean CT−$^1L_a$ energy gap, the quantum yield is determined using the Boltzmann factor

$$\Phi_f = \frac{k_r}{k_r + k_{nr}} \exp\left(\frac{-(E_{CT} - E_{1La})}{k_B T}\right) \quad (3)$$

In this paper, only the ribonuclease T1 (RNT) point in Figure 1 was placed in this manner.

**Calculation of Quenching by the Histidine Cation.** The QM chromophore used is the same as that for amide quenching but with the addition of a histidine cation, not covalently attached. The following scheme, using a combination of experimental and ab initio quantum computations on 3MI and $4MIm^+$, was used to structure our procedure for estimating the fluorescence quenching rate by $His^+$[30,31]

$$3MI(G) \rightarrow 3MI^{\bullet+}(CT) + e^- \qquad 7.54 \text{ eV (exp)}$$

$$4MIm^+(G) + e^- \rightarrow 4MIm^{\bullet}(CT)$$

$$-4.52 \text{ eV (ab initio)}$$

$$3MI^*(La) \rightarrow 3MI(G) + h\nu \qquad -4.39 \text{ eV (exp)}$$


dx.doi.org/10.1021/jp211217w | J. Phys. Chem. B 2012, 116, 2586−2594

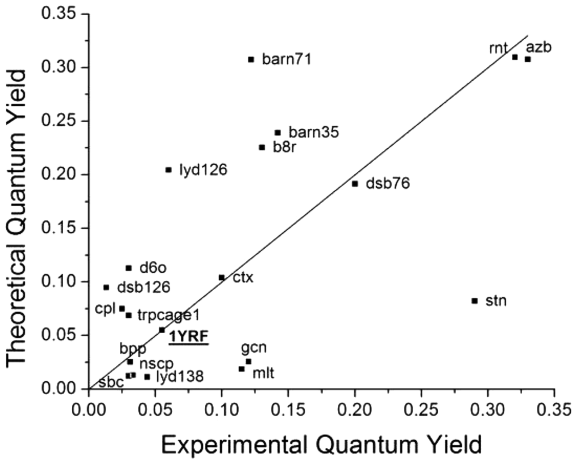


**Figure 1.** Plot of calculated versus experimental fluorescence quantum yields for 20 Trps in 17 different single-Trp proteins.

which sum to

$$3MI^*(La) + 4MIm^+(G) \rightarrow 3MI^{\bullet+}(CT) + 4MIm^{\bullet}(CT) \qquad -1.37\ eV = -11\,000\ cm^{-1}$$

The observed adiabatic ionization potential for 3MI[30] is predicted within 0.01 eV using B3LYP/6-311+G(2df,2p), as calibrated with several known IPs.[30] We have used the same procedure to extrapolate a value of 4.52 eV for the electron affinity of the $4MIm^+$ ring in vacuum.

The $-11\,000\ cm^{-1}$ value for the adiabatic energy gap in vacuum is to be compared to Zindo calculations using the coordinates from the MD, in which the Trp and $His^+$ rings are in the ground-state geometry and the calculated CT$-{}^1L_a$ energy gap is vertical. We find that by using the OPLS force field ground-state (G) geometries for the Trp and $His^+$ rings, the Zindo (Z) computed CT$-{}^1L_a$ gaps are $\sim -12\,000\ cm^{-1}$ in vacuum

$$3MI^*(G, MD, Z) + 4MIm^+(G, MD, Z) \rightarrow 3MI^{\bullet+}(G, MD, Z) + 4MIm^{\bullet}(G, MD, Z) \qquad -1.66\ eV = -12\,000\ cm^{-1}$$

This scheme suggests that by adding $1000\ cm^{-1}$ to the computed vertical Zindo energy gap, we would predict the desired adiabatic gap, provided the electrostatic contribution estimated from the surroundings as approximated by the force field point charges is accurate. As with the amide quenching, we are forced to add an empirical offset that provides a reasonable fit of the predicted quantum yield to experiment. For the purposes of this paper, we connect to experiment through the published fluorescence quantum yield of Trp94 in the protein barnase, which is stacked against His18 in much the same way as Trp23 is to His27 in villin for what we will call the "close" conformation. Unlike the villin case, the Trp$-His^+$ distance is nearly constant during our simulations (not shown). At low pH, $\Phi_f$ for a mutant containing only Trp94 is 0.017.[32] This quantum yield is consistent with a $1.8 \times 10^9\ s^{-1}$ quenching rate and requires that we add $9000\ cm^{-1}$ to the Zindo value when using the OPLS force field. We attribute this difference to some inaccuracy in the Zindo numbers and in the electrostatic effect of the point charge environment, which we find varies with the force field.

Calibrating for $His^+$ quenching was done by assuming that the fluorescence quenching to amide is independent of the protonation state of $His^+$ in HP35, a conclusion based on simulations of HP35 with a neutral His and of the 36-residue original WT protein (HP-36) with asparagine at position 27, both of which gave very similar calculated amide fluorescence quenching rates as that for HP35 with protonated His.[33]

The method of calculating the quantum yield must take into account the heterogeneity (and possibly associated interconversion rates) found in our simulations in which fast quenching by $His^+$ ($2 \times 10^9\ s^{-1}$) occurs only transiently during certain rotamer states that bring the Trp and $His^+$ into close proximity. The method that we have used to predict quantum yields is described in the Results section and in Supporting Information.

**Electrostatic Energy Shifts from Solvent and Protein.** These are calculated using the formula

$$\Delta E_{env} = \sum_{\alpha} V_{\alpha} \Delta \rho_{\alpha} \tag{4}$$

Where $\Delta E_{env}$ is the vertical Coulombic electrostatic energy difference between the CT and ${}^1L_a$ state, $V_\alpha$ is the Coulomb potential, and $\Delta\rho_\alpha$ is the charge difference at the $\alpha$th quantum atom associated with the ${}^1L_a \rightarrow$ CT state.

$V_\alpha$ is defined as

$$V_{\alpha} = \sum_{k} \frac{q_k}{4\pi\varepsilon_0 r_{\alpha,k}} \tag{5}$$

where $q_k$ is the charge at the $k$th nonquantum atom and $r_{\alpha,k}$ is the distance between the $k$th nonquantum atom and the $\alpha$th quantum atom.

By restricting the $k$ and $\alpha$ indices appropriately, one may estimate the major electrostatic contributions from any part of the environment for any of the possible quenching ETs.

## RESULTS

**Amide Quenching.** Figure 1 shows results from extending our previous work on 20 single-Trp proteins[20] to longer simulations and using GROMACS with the OPLS force field. The overall fit is comparable to our previously published fits.[17,18,20] Quenching by amide is quite competitive with that from $His^+$ when averaged over time, in agreement with what can be inferred from experimental observations of the quantum yield for HP35 at pH 7[33] and WT villin at any pH.[33] In contrast to quenching by $His^+$, however, the CT$-{}^1L_a$ gap and computed quenching rate are virtually constant throughout the trajectories that we have carried out.

**Tryptophan–Histidine Distance and Quenching.** Figures 2–5 contain trajectories of properties computed from four $\sim$1 $\mu$s MD simulations performed on the villin headpiece with explicit water involving an eclectic sample of mutants, force fields, and temperatures. Figures 2 and 3 compare HP35(N27H) using the OPLS and AMBER-SB-ILDN force fields at 300 K; Figures 2 and 4 compare HP35 and 2F4K using OPLS at 300 K; and Figures 2 and 5 compare HP35 folded at 300 K and unfolded at 400 K using OPLS.

Figures 2a, 3b, 4a, and 5a show trajectories of the distance between the Trp23 and $His^+27$ centers of mass (COM) derived from the corresponding simulations. This distance is considered the best single indicator of the quenching rate of Trp fluorescence by $His^+$.[6,7] All four trajectories exhibit a similar behavior, marked by several regions of discrete inter-residue distance. Most striking and significant is the small percentage of


dx.doi.org/10.1021/jp211217w | J. Phys. Chem. B 2012, 116, 2586–2594

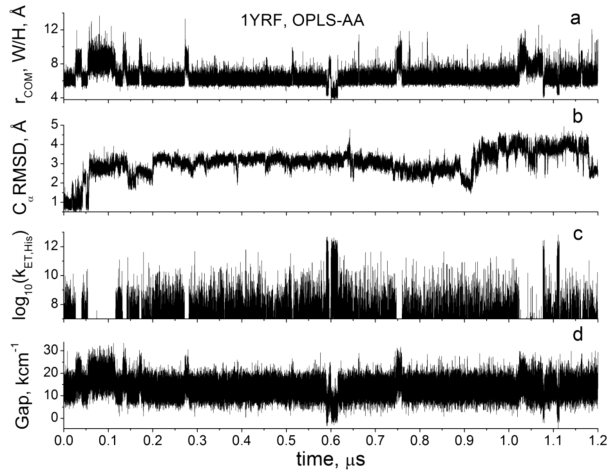


**Figure 2.** A 1 $\mu$s simulation of HP35(N27H$^+$) with the OPLS-AA force field. (a) Center of mass (COM) distance between Trp (W) and His$^+$ (H) rings, (b) C$_\alpha$ rmsd relative to the crystal structure (PDB = 1YRF), (c) calculated ET rate, s$^{-1}$, for quenching by His$^+$, and (d) CT(His$^+$)−$^1$L$_a$ energy gap from MD and Zindo. Note the significant correlation between distance, rate, and energy gap, but note also that there is no correlation between the rmsd and quenching ability for His$^+$. In this simulation, quenching occurs only during the brief periods in which a rotamer switch brings the COM of the rings within <5.5 Å.

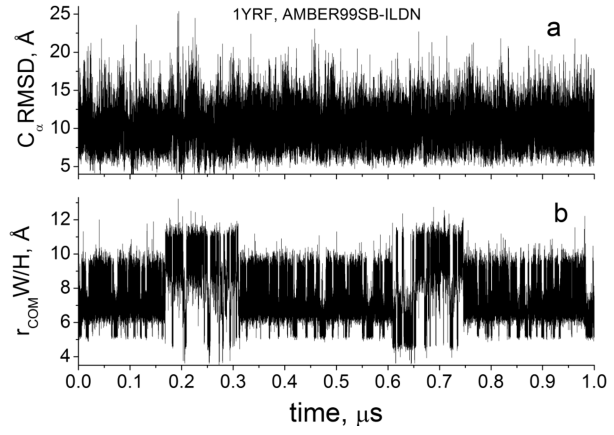


**Figure 3.** A 1 $\mu$s simulation of HP35(N27H$^+$) with the AMBER-SB-ILDN force field. (a) C$_\alpha$ rmsd relative to crystal structure (PDB = 1YRF). (b) Center of mass (COM) distance between Trp (W) and His$^+$ (H) rings. Again, quenching occurs only during the brief periods in which a rotamer switch brings the COM of the rings within <5.5 Å.

time for which the closest distance (~4 Å) is visited during the three trajectories of folded villin (Figures 2−4), while this region is helical 100% of the time according to the backbone rmsd. We find that in all cases, the close distance state arises solely through a concerted $\chi_1$ and $\chi_2$ transition, an example of which is shown in Figure 4b and c. The close conformation is achieved only if $\chi_1$ is ~180° and $\chi_2$ is ~+90°. The vast majority of the time, $\chi_1$ is ~+60° and $\chi_2$ is ~-90°. See Figure S1 (Supporting Information) for a graphical representation of these structures.

Figure 2c shows how the computed quenching rate constant varies with time during the trajectory. Note the strong correlation of the Trp−His$^+$ distance with quenching rate. For reference, if the quenching rate drops below 1 × 10$^7$ s$^{-1}$, there is negligible effect on the quantum yield. Figure 2d shows that the important energy gap between the CT state and $^1$L$_a$

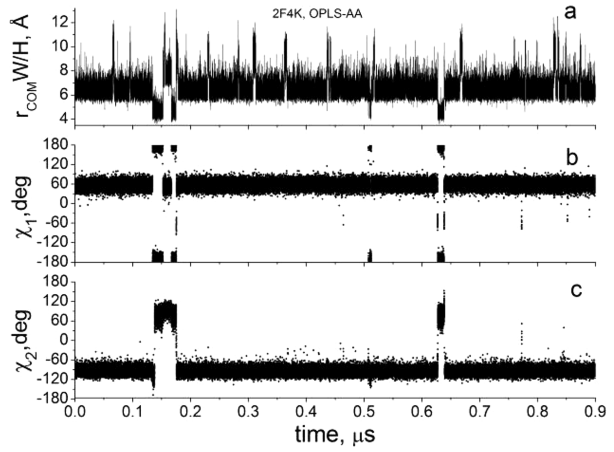


**Figure 4.** A 0.9 $\mu$s simulation of HP35(N27H$^+$,K24Nle,K29Nle) with the OPLS-AA force field showing correlation with Trp dihedral angles, $\chi_1$ and $\chi_2$ . As in Figures 2 and 3, quenching occurs only during the brief periods in which a rotamer switch brings the COM of the rings within <5.5 Å. (a) COM distance between Trp (W) and His$^+$ (H) rings. (b) Trp23$_{\chi 1}$ versus time. and (c) Trp23$_{\chi 2}$ versus time.

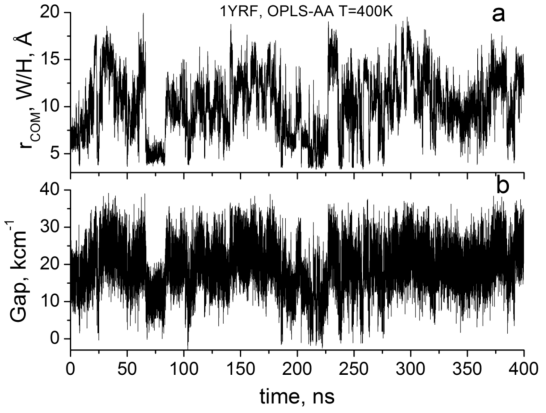


**Figure 5.** A 400 ns simulation at 400 K of unfolded villin HP35 (N27H) showing strong correlation of the CT−$^1$L$_a$ energy gap with distance. The same correlation is seen in Figure 2 and is present in the trajectories of Figures 3 and 4 (not shown). (a) COM distance between Trp (W) and His$^+$ (H) rings and (b) His$^+$ CT−$^1$L$_a$ energy gap versus time.

has an unexpected strong correlation with Trp−His$^+$ distance. This also has a profound effect on the quenching rate. Surprisingly, much the same frequency of occurrence of the short distance is found for a simulation of completely unfolded villin at 400 K (Figure 5a). The current assumption by experimentalists and computationalists alike is that when the region encompassing these two residues is helical, there will be significant quenching, but there will be no quenching otherwise. We will show later in this section that the thermodynamics and kinetics of this switching can provide a mechanism for Trp fluorescence to report the global folding rate and also account for the observed multiexponential unfolding kinetics.

**Important Role of Histidine Cation Solvation.** The unanticipated strong correlation of the His$^+$ CT−$^1$L$_a$ vertical energy gap versus distance, seen in Figures 2d and 5b, is also present for the simulations of Figures 3 and 4 (not shown). While such a correlation is expected for ET between the neutral donor and acceptor due to the Coulombic stabilization between the radical ions produced, ET from the neutral Trp to the His


dx.doi.org/10.1021/jp211217w | J. Phys. Chem. B 2012, 116, 2586−2594

cation does not yield a large difference in Coulombic interaction between the donor and acceptor upon ET in vacuum. We find that the source of the strong correlation lies primarily in a large change in solvation energy at short distance compared to that at longer distances. At large separation, the vertical CT energy immediately after ET is highly destabilized by the polarization of the water oriented by the His cation prior to ET. This destabilization decreases sharply when the separation is small enough to exclude water in the region between the donor and acceptor. The energy gap is the key variable in the FCDOS, which in turn is a major factor in the Fermi rule for the ET rate and is a measure of the extent of resonance of the CT state with the emitting state. Figure 6 shows how the FCDOS and,

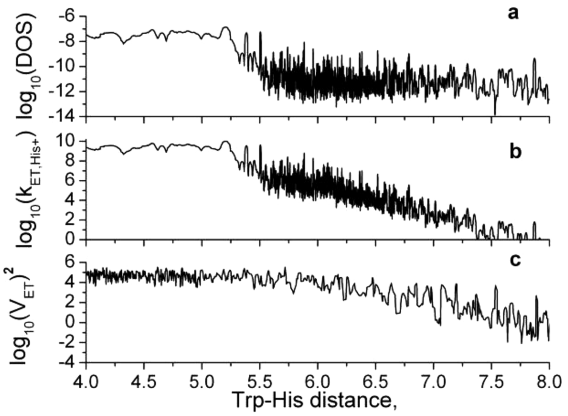


**Figure 6.** $\text{Log}_{10}$ plot versus Trp−$\text{His}^+$ COM distance of (a) Franck−Condon weighted density of states, in units of states per $\text{cm}^{-1}$ (FCDOS); (b) the Fermi-rule-calculated ET rate constant for Trp → $\text{His}^+$ in units of $\text{s}^{-1}$ ; and (c) the square of the ET Hamiltonian matrix element ($V_{ET}$) for coupling fluorescing and the histidine CT state in units of $(\text{cm}^{-1})^2$.

accordingly, the Fermi-rule-computed ET rate constant drop sharply by 3 orders of magnitude as the distance increases from 4 to 5.5 Å. Note that in this distance range, we find that the average square of electronic coupling in the Fermi rule changes very little, contrary to usual assumptions and experimental findings at larger distances. Similar deviation at short distance has been reported previously.[34,35]

The picture that emerges from the results presented above is that quenching by $\text{His}^+$ happens almost exclusively at the closest distance. The duration of the close state typically exceeds the excited-state lifetime of Trp, meaning that the fluorescence intensity will exhibit heterogeneity. In other words, there are in effect two species, one in which the quenching rate is fast by $\text{His}^+$ and one in which the quenching is moderate from amide. This is seen in Figure 6 by realizing that when the distance exceeds ~5.2 Å, the effect of $\text{His}^+$ quenching drops below $10^7$ $\text{s}^{-1}$ and becomes negligible compared to amide quenching and the non-ET decay channels.

**His−Trp Distance versus rmsd.** Comparing the Trp−$\text{His}^+$ distance with $C_\alpha$ rmsd shows different behaviors depending on the nature of the force field. Using OPLS-AA, helix III unzipped continuously throughout the trajectory, with a corresponding increase in the rmsd, as seen in Figure 2b. The Trp−$\text{His}^+$ distance was independent of this, however, because the helix was intact between Trp and $\text{His}^+$ during the entire trajectory. Using AMBERSB99-ILDN, helix III was completely formed during the entire trajectory, except for Phe35, which is consistent with a low constant rmsd throughout. For 2F4K using OPLS-AA, the 25−29 backbone H-bond of helix III was fully formed during the entire trajectory, but that of 26−30 was ~6 Å during the entire trajectory. For these three essentially 100% folded villin structures, the rmsd and Trp−$\text{His}^+$ distance are not correlated.

**Calculation of Quantum Yields and Lifetimes: The Effect of Heterogeneity.** The heterogeneity predicted from the simulations has a profound effect on how the quantum yield is to be calculated. Two "species" are identified, one designated "F" in which Trp and $\text{His}^+$ are far apart and too distant for quenching by $\text{His}^+$ and one designated "C" in which Trp and $\text{His}^+$ are close, between 4 and 5 Å, for which Trp is quenched by ET to $\text{His}^+$. There are two obvious extremes. When interconversion between the rapidly quenched close species and slowly quenched far species is much slower than the Trp fluorescence lifetime of either species, the quantum yield is given simply by the average of the individual quantum yields

$$\Phi_{\text{slow exchange}} = f_C\Phi_C + f_F\Phi_F \tag{6}$$

where $f_C$ and $f_F$ are the fractions of time spent in the close and far conformations. At the other extreme, when the two species exchange at rates much faster than the fluorescence decay rate, the quantum yield becomes

$$\Phi_{\text{fast exchange}} = \frac{k_r}{k_r + k_{nr} + f_C(k_{ET,Am} + k_{ET,His^+}) + f_F k_{ET,Am}} \tag{7}$$

Even when $f_C \ll f_F$, if $k_{ET,His^+}$ is large enough, the quantum yield can become very small because the rapidly depleted close species will be replenished by the fast exchange process.

The simulations reported here and elsewhere[6] suggest that the exchange rate between the two species may approach the fluorescence decay rate, conditions under which the two limits just mentioned will be in considerable error. In this intermediate region, we expect to see two lifetimes that are not the pure lifetimes of each of the species. To explore this behavior, we perform a simple compartmental analysis consisting of four fluorescing states connected by rate constants shown in Figure 7, folded far (FF), folded close (FC), unfolded far (UF), and unfolded close (UC). Also in this scheme, GS stands for that part of an initially excited state population that has returned to the ground state. This type of analysis has been used in numerous applications to multiple fluorescent species with somewhat different focus and emphasis.[36−38] First, we consider only the fluorescence dynamics of the folded state, that is, the upper half of Figure 7. The decay rates out of the two excited species are

$$k_{DF} = k_r + k_{nr} + k_{ET,Am}$$
$$k_{DC} = k_r + k_{nr} + k_{ET,Am} + k_{ET,His^+} \tag{8}$$

where $k_r$, $k_{nr}$, $k_{ET,Am}$, and $k_{ET,His^+}$ are the radiative, nonradiative, ET to amide, and ET to histidine rate constants, respectively. The coupled rate equations generated from the folded part of Figure 7 were solved by standard procedures. Details are given in the Supporting Information.

Figure 8 shows an example of how the quantum yield changes as the exchange rate, $k_{ex}$, increases without altering the equilibrium between species FF and FC for the special case of $k_{FF,FC} = k_{FC,FF} = k_{ex}$, $k_{ET,Am} = 0.5$ $\text{ns}^{-1}$, and $k_{ET,His^+} = 2$ $\text{ns}^{-1}$,


dx.doi.org/10.1021/jp211217w | J. Phys. Chem. B 2012, 116, 2586−2594

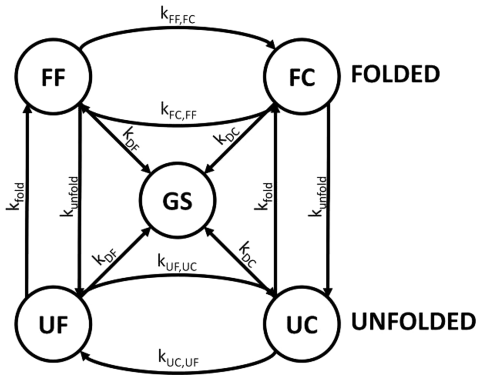


**Figure 7.** Kinetic model for calculating tryptophan fluorescence quantum yields as a function of temperature in the case of lifetime heterogeneity involving a close conformation in which $His^+$ can quench Trp fluorescence and a far conformation where quenching is only by the amide. The species with Trp excited are as follows: FF = folded far, FC = folded close, UF = unfolded far, and UC = unfolded close; GS = that portion of the excited population that has returned to the ground state. Far and close refer to the distance between Trp and $His^+$. Quenching of Trp by $His^+$ only occurs in the close conformation.

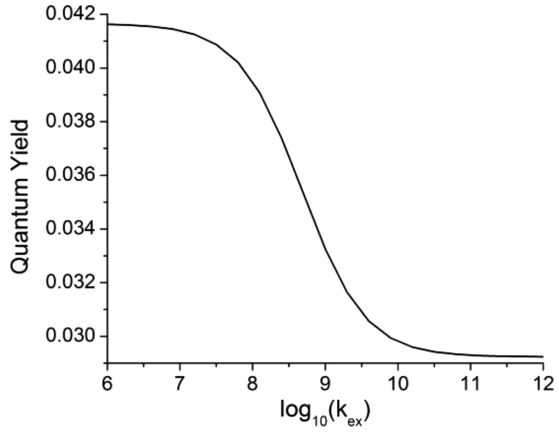


**Figure 8.** Example of the fluorescence quantum yield Φ in the folded state as a function of the exchange rate, $k_{ex} = k_{FF,FC} = k_{F,FF}$, for interchange between the far and close conformations for a specific case in which $k_{FF,FC} = k_{FC,FF}$, $k_{DF} = 0.62\ ns^{-1}$, and $k_{DC} = 2.12\ ns^{-1}$. Note that the quantum yield starts to deviate at exchange rates that are close to the slow fluorescence decay rate in the far conformation, $k_{DF} = 5 \times 10^8\ s^{-1}$.

which we believe is representative of the fluorescence of tryptophan in HP-35. Figure 9 illustrates how the normalized amplitudes and the lifetimes for the two exponential terms in the time-resolved fluorescence change as a function of the rate of exchange, $k_{ex}$, between the far and close species in this special case. A more general presentation of the quantum yield behavior as a contour plot in terms of $\log_{10}(K_{eq}) = \log_{10}([FC]/[FF])$ and $\log_{10}(k_{FF,FC} + k_{FC,FF}) = \log_{10}(k_{relax})$ is shown in Figure 10. The quantum yield magnitude is given by color on the right. Moving vertically on this graph (increasing the sum of the forward and backward exchange rate constants), each contour line crossed indicates a decrease in quantum yield by 0.0025. Moving horizontally left to right on this graph (increasing the ratio of the close to the far populations), each contour line crossed also indicates a decrease in quantum yield by 0.0025.

**Modeling of Temperature Jump Experiments.** Because our simulations consistently show that the Trp fluorescence

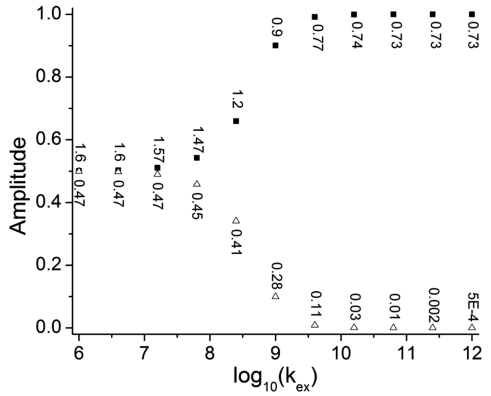


**Figure 9.** Transition from the slow exchange limit (pure heterogeneity) to the fast exchange limit as function of $\log_{10}(k_{ex})$; $k_{ex}$ is defined in the Figure 8 caption. The vertical axis gives the fractional amplitudes of the long-lifetime (upper curve, filled squares) and short-lifetime (lower curve, open triangles) exponentials, whose corresponding lifetimes in nanoseconds are shown as numbers attached to the points. Note that in the presence of interconversion between the species, there is no direct correspondence between the "species" and the "lifetimes". As the exchange rate increases, the two lifetimes evolve ultimately to a single average lifetime that applies to both species and an extremely fast transient corresponding to establishing a steady state following a delta function excitation pulse.

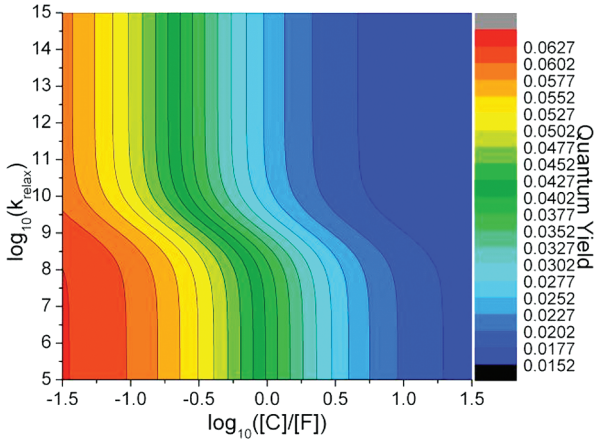


**Figure 10.** Contour graph of the quantum yield as a general function of $\log_{10}(k_{relax}) = k_{FF,FC} + k_{FC,FF}$ and the equilibrium constant $K_{eq}$ = [Close]/[Far]. Contour lines are separated by quantum yield increments of 0.0025.

quantum yield is drastically changed by a transient rotamer transition with no significant helix unfolding, a new interpretation of the 70 ns exponential term found by Kubelka et al.[10] in temperature jump relaxation experiments presents itself. We propose that the fast relaxation stems from a shift of population of the close and far populations and that the sum of the exchange rate constants, $k_{FF,FC} + k_{FC,FF}$, is $\sim(70\ ns)^{-1}$, the experimental value.[10] In addition, we extend the kinetic equations to include the unfolded protein part of Figure 7, to which we also ascribe a far and close species UF and UC with $k_{fold}$ and $k_{unfold}$ as a function of temperature, taken directly from kinetic data fitting by Kubelka et al.[10] For simplicity, we take the fluorescence decay constants $k_{DF}$ and $k_{DC}$ to be the same as those in the folded state. We do not, however, simulate the extreme decrease of quantum yield with increasing temperature, which is a property of the bare Trp chromophore only.[26] $k_{UF,UC}$


dx.doi.org/10.1021/jp211217w | J. Phys. Chem. B 2012, 116, 2586–2594

+ $k_{UC,UF}$ was also made equal to $(70\ ns)^{-1}$ with no temperature dependence. See the Supporting Information for details. Figure 11

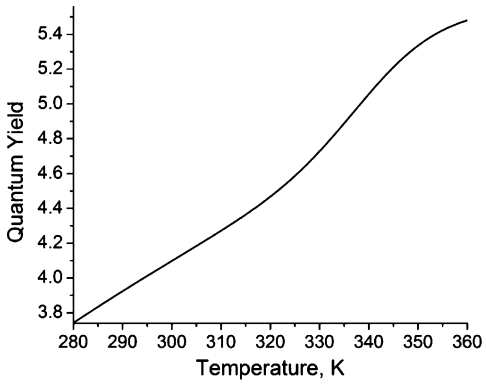


**Figure 11.** Unfolding versus temperature using the scheme of Figure 7 with experimental folding and unfolding rates from Kubelka et al. (2003).[10] The values used in the model are in Table S1 (Supporting Information). The large temperature dependence of internal non-radiative loss of the Trp ring (independent of folding) is not included in the model. The slower rise preceding the unfolding transition is from the shifting equilibrium between the close and far conformations.

shows a plot of the quantum yield versus temperature, modeled using the parameters of Table S1 of the Supporting Information. This plot exhibits the features seen in the corresponding experimental curve. With these parameters, it is also possible to simulate temperature jump experiments. The observed amplitude and temperature dependence is achieved with $\Delta H^0_{FC} = -2.4$ kcal/mol for the far → close transition. Figure 12 shows such a result for

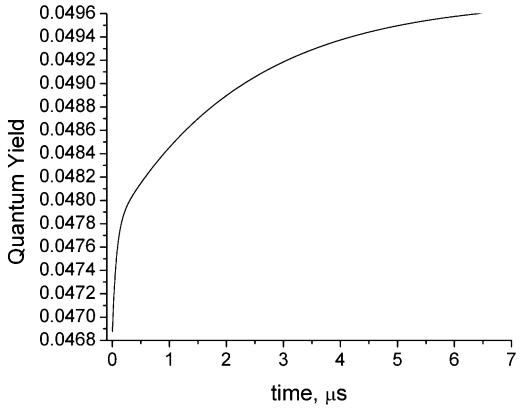


**Figure 12.** Time trace for the model of the fluorescence quantum yield from Figure 11 and Table S1 (Supporting Information) after a temperature jump from 328 to 337 K.

a 9 K temperature jump starting at 328 K. The trace shows the two expected relaxation times, a fast ~70 ns rise caused by re-equilibration between the far and close configurations in the folded state and the 5 $\mu$s rise, which is the sum of $k_{fold}$ and $k_{unfold}$ from Kubelka et al.[10]

## DISCUSSION

**How Trp23 Fluorescence Can Report Global Folding.** Until now, the model for how Trp fluorescence of villin is affected by folding has been an "all or nothing" picture; Trp23 is quenched if (and only if) helix III is formed.[5−7] Ensign et al.[7] were able to create a reasonable approximation to a folding ensemble from hundreds of microsecond-scale simulations. The authors compared two models, a surrogate model of fluorescence-detected folding, in which fluorescence is quenched only if the Trp−$His^+$ distance is <7.5 Å, and a structural metric for folding that defines the folded state as having all three helices folded and the three core phenylalanine contacts present. By either metric, a broad spectrum of folding times was found, with the surrogate fluorescence model generally predicting shorter folding times. In the multiple-microsecond simulations of Freddolino and Schulten,[6] the discrete nature of the Trp−$His^+$ distance is prominent, and the close distance, which we believe is the only quenching configuration, was in each case observed at times < 0.6 $\mu$s. Both papers strongly suggested that Trp 23 fluorescence may be biased to shorter folding times because helix III may fold on average well before the protein is completely folded, in contrast to recent experimental results.[9,14]

The heterogeneity of the fluorescence quenching seen in our simulations provides a possible mechanism by which the quantum yield is more finely tuned. The relatively high quenching rate ($1.8 \times 10^9\ s^{-1}$) in the close state inferred from the quantum yield of Trp 94 of barnase at low pH (0.017)[32] means that small changes in the population of the close state can have a large impact on the quantum yield. At high pH, $\Phi_f$ = 0.07 for barnase[32] and 0.055 for HP35.[33] Lowering the pH from 7.4 to 4.9 at 300 K for folded HP35 lowers $\Phi_f$ from 0.055 to 0.04 using the rate derived from low pH barnase if ~40% close conformation is assumed. See the Supporting Information for an overview of the tryptophan fluorescence details pertinent here.

The simulations presented in Figures 2−4 suggest that the fraction in the close conformation may be nearer to 5 than 40%, but we hasten to point out that an error of only 1.5 kcal/mol for $\Delta G^0$ for the far → close transition predicted by the MD would account for this apparent discrepancy. We use this fact to infer that subtle changes of only 1−2 kcal/mol for the conversion of the far to the close species would substantially modulate the fluorescence quantum yield, and therefore, we postulate that measurable quantum yield variations due to subtle changes in the environment of helix III in the incompletely folded intermediates will be observable. This provides a mechanism by which Trp fluorescence can report the global folding rate.

As a tangible example of such subtle changes, consider the final folding step studied extensively by Freddolino and Schulten.[6] In each of the simulations for which the fully folded state was reached, a long-lived prefolded intermediate was reached in which all three helices were fully formed, but helix I was flipped and rotated relative to the fully folded state. In this intermediate, the hydrophobic face of helix I was seen to be directed toward solvent or helix II, with its hydrophilic face closer to helix III. This state allows salt bridges involving D3-K24 and K7-E31 between helices I and III, which are not possible in the correctly folded state. In addition, a number of other salt bridges were seen[6] to form transiently between the lysines of helix III (K24, K29, K32) and the acidic residues on helix I (D3, E4, D5); some combination of these interactions occurs in the flipped state in all WT trajectories.[6] We have noted that Lys24 forms a "cation−$\pi$" and/or hydrophobic stacking with Trp27 for long periods of the trajectories but is disrupted during the brief rotamer states that allow the close contact conformation. Plausibly, a salt bridge involving Lys24

would perturb the rate of exchange and population of the quenched state.

**Is Helix III Disordered in the Folded State?** Whether the above scheme has merit depends crucially on the question of how the 70 ns transient is assigned. At the center of the question that we wish to answer is whether helix III is partially unwound in the native state. The TTET experiments of Kiefhaber and co-workers[14] indicate fast contact between positions 23 and 35 even at 5 °C and no denaturant. This they take as evidence for unraveling of helix III, even in the folded state. In our simulations, the answer to this question depends on which force field we use. Our three 1 $\mu$s simulations vary distinctly in the extent of helix III unwinding, but in all three, the short section of the helix involving Trp23 and His27 remains intact. This is true even for HP35 using the OPLS force field, wherein the increasing $C_\alpha$ rmsd seen in Figure 2b is almost entirely due to a steadily increasing degree of helix III unwinding. Remarkably, using AMBER99SB-ILDN, where helix III is intact except for the C-terminal residue, Phe35, the length of the xanthene triplet donor used in the TTET experiments in place of Phe35 allows for contact with the acceptor at position 23, despite the helix being virtually intact. Saladino et al.[39] have recently noted that for HP36 during unbiased simulations using AMBER99SB-ILDN, Phe35 comes within ∼9 Å of Trp35. This is also consistent with the analysis of Beauchamp et al.[15] showing that position 34 has an order of magnitude lower frequency of contact with Trp23 than does Phe35. Whether the TTET result is definitive in exposing anything but minor unzipping of helix III in the folded state is therefore not so clear.

**Exchange Rate.** The concept of pure heterogeneity requires that interconversion between the species be much slower than the rate of fluorescence decay. The simulations of Freddolino and Schulten[6] suggest that residence times are on the order of 50−200 ns, which obeys the criterion for pure heterogeneity. The simulations shown here in Figures 2−4 suggest that the residence time for the close conformation may be on the order of the excited-state lifetime, but these simulations are too short to be statistically significant. Figures 8−10, however, illustrate how sensitive the quantum yield and lifetime can be if there are intermediate structures for which the exchange relaxation approaches $1 \times 10^8$ $s^{-1}$.

**Unfolded Villin at 400 K.** We were surprised to find that the amount of close Trp−$His^+$ contact seen in our simulation at 400 K (Figure 5) is similar to that for folded HP35 and 2F4K at 300 K. This is, however, consistent with the 100 $\mu$s simulations of Piana et al.[16] using different force fields, which found that residues in helices spend from 44 to 90% of the time in helix form in the unfolded state at their computed melting temperatures. This raises the possibility of considerable quenching by $His^+$ even in the unfolded state, which might be another reason that the change in quantum yield is so modest.

**On SASA as a Surrogate for Fluorescence Quantum Yield.** The solvent-accessible surface area (SASA) is reasonably used as one of several metrics for the extent of folding[16] and has been suggested as a surrogate for the fluorescence quantum yield ($\Phi_f$).[16] In our simulations, however, we find no time correlation of our computed quenching rate with SASA, except during the two transient periods of the double rotamer transition, in which Lys24 simultaneously becomes separated from the face of the Trp ring (see Figure S2, Supporting Information).

In our opinion, SASA is not a reliable surrogate for fluorescence quenching in general. If one is monitoring the fluorescence quantum yield and the quenching is by amide, different cases are possible. For completely buried Trps with a maximal quantum yield (∼0.3), denaturing virtually always leads to quantum yield reduction. This is because when water hydrogen bonds as a donor to the amide carbonyl O and as an acceptor to the Trp ring HN, the amide CT state is lowered in energy, causing a greater quenching rate. The opposite is true in many cases, however. For the conserved Trps in the Crystallin proteins of the eye lens, unfolding leads to 10−20-fold increases of the quantum yield because the electrostatic environment in the folded proteins promotes faster quenching. There, much of the quenching is enhanced by two waters that are buried with the Trp.[40] Increased SASA in such cases would correlate with increased fluorescence. Similarly, if one is using the fluorescence $\lambda_{max}$, typically greater SASA gives a longer wavelength and would almost always correlate with unfolding for a buried Trp.

For histidine cation quenching, SASA of $His^+$ (instead of Trp) would appear to be the best mimic, according to the findings of this paper. Our calculations say that quenching by a fully solvated histidine cation is not possible and becomes possible only when $His^+$ is so close to the Trp that water is not in contact with the face of the $His^+$ stacked near the Trp. However, His27 spends a considerable time salt bridged with Glu31, which could also modulate the SASA of $His^+$.

Finally, we note that fluctuations in several seemingly disparate properties of single proteins, including switching between neutral and anionic forms of near-denatured green fluorescent protein, spectral diffusion, fluorescence lifetimes, and enzyme catalysis rate constants, all exhibit nearly the same correlation functions.[41,42] Prakash and Marcus have shown that the origin of this commonality may lie in their finding that the more fundamental fluctuations of the electrostatic energy and dielectric susceptibility also exhibit this same correlation behavior. It is therefore unclear whether specific cause and effect conclusions from such correlation functions can be made.

## ■ CONCLUSIONS

The principal finding of this work is that even while helix III is formed, much of the time $His^+27$ does not quench fluorescence from Trp23. Our calculations (as calibrated with Trp94 of barnase) say that quenching happens only during certain periods in the folded helical state when specific rotamer conformations bring Trp and $His^+$ into close contact, a contact distance substantially closer than that in the crystal structure. Quenching is not possible at longer distances because the energy of the CT state responsible for quenching by $His^+$ is greatly destabilized by greater solvation of $His^+$, taking the CT state out of resonance with the fluorescing state. The resulting heterogeneity regarding the fluorescence signal, in which there are effectively two species, means that small changes in the fraction of the highly quenched species (corresponding to ∼1 kcal/mol in $\Delta G^0$) or in the rate in which the two species exchange, will have a measurable effect on the average quantum yield. This in turn means that intermediate unfolded structures with helix III fully intact may have different quantum yields, thereby providing a mechanism by which Trp fluorescence should be able to reliably report the global folding rate, despite early folding of helix III.

In addition, the 70 ns relaxation time reported by Kubelka et al.[10] is consistent with the rate of exchange between the close

and far conformations in our simulations if we impose a temperature dependence of the equilibrium between the close and far conformations of the helical structure arising from a small negative $\Delta H^0$ associated with forming the close conformation.

## ■ ASSOCIATED CONTENT

### Supporting Information

(1) Figure showing quenching and nonquenching Trp−$His^+$ configurations; (2) pertinent tryptophan fluorescence principles; (3) equations supporting Figures 8−12; and (4) figure showing noncorrelation of SASA with computed fluorescence quenching. This material is available free of charge via the Internet at http://pubs.acs.org.

## ■ AUTHOR INFORMATION

### Corresponding Author

*E-mail: pcallis@montana.edu. Fax: (406) 994-5407.

### Notes

The authors declare no competing financial interest.

## ■ ACKNOWLEDGMENTS

This work was supported by NSF Grants MCB-0446542 and MCB-0847047, and Teragrid/XSEDE grants TRAC MCB090176 for (2009-2011). We thank Drs. William Eaton and Vijay Pande for encouraging this work, and Dr. Jan Kubelka for providing quantum yield data.

## ■ REFERENCES

(1) Eftink, M. R. *Methods Biochem. Anal.* **1991**, *35*, 127−205.
(2) Royer, C. A. *Chem. Rev.* **2006**, *106*, 1769−1784.
(3) Ross, J. B. A.; Laws, W. R.; Shea,M. A. In *Protein Structures: Methods in Protein Structure and Structure Analysis*; Uversky, V., Permyakov, E. A., Eds.; Nova Science Publishers, Inc.: New York, 2007; pp 1−18.
(4) Buchner, G. S.; Murphy, R. D.; Buchete, N. V.; Kubelka, J. *Biochim. Biophys. Acta* **2011**, *1814*, 1001−1020.
(5) Kubelka, J.; Henry, E. R.; Cellmer, T.; Hofrichter, J.; Eaton, W. A. *Proc. Natl. Acad.Sci. U.S.A.* **2008**, *105*, 18655−18662.
(6) Freddolino, P. L.; Schulten, K. *Biophys. J.* **2009**, *97*, 2338−47.
(7) Ensign, D. L.; Kasson, P. M.; Pande, V. S. *J. Mol. Biol.* **2007**, *374*, 806−816.
(8) Kubelka, J.; Chiu, T. K.; Davies, D. R.; Eaton, W. A.; Hofrichter, J. *J. Mol. Biol.* **2006**, *359*, 546−553.
(9) Cellmer, T.; Buscaglia, M.; Henry, E. R.; Hofrichter, J.; Eaton, W. A. *Proc. Natl. Acad. Sci. U.S.A.* **2011**, *108*, 6103−6108.
(10) Kubelka, J.; Eaton, W. A.; Hofrichter, J. *J. Mol. Biol.* **2003**, *329*, 625−630.
(11) Thompson, P. A.; Munoz, V.; Jas, G. S.; Henry, E. R.; Eaton, W. A.; Hofrichter, J. *J. Phys. Chem. B* **2000**, *104*, 378−389.
(12) Eaton, W. A.; Munoz, V.; Thompson, P. A.; Henry, E. R.; Hofrichter, J. *Acc. Chem. Res.* **1998**, *31*, 745−753.
(13) Mohammed, O. F.; Jas, G. S.; Lin, M. M.; Zewail, A. H. *Angew. Chem., Int. Ed.* **2009**, *48*, 5628−5632.
(14) Reiner, A.; Henklein, P.; Kiefhaber, T. *Proc. Natl. Acad. Sci. U.S.A.* **2010**, *107*, 4955−4960.
(15) Beauchamp, K. A.; Ensign, D. L.; Das, R.; Pande, V. S. *Proc. Natl. Acad. Sci. U.S.A.* **2011**, *108*, 12734−12739.
(16) Piana, S.; Lindorff-Larsen, K.; Shaw, D. E. *Biophys. J.* **2011**, *100*, L47−L49.
(17) Callis, P. R.; Vivian, J. T. *Chem. Phys. Lett.* **2003**, *369*, 409−414.
(18) Callis, P. R.; Liu, T. *J. Phys. Chem. B* **2004**, *108*, 4248−4259.
(19) Callis, P. R.; Liu, T. Q. *Chem. Phys.* **2006**, *326*, 230−239.
(20) Callis, P. R.; Petrenko, A.; Muino, P. L.; Tusell, J. R. *J. Phys. Chem. B* **2007**, *111*, 10335−10339.
(21) Callis, P. R. In *Reviews in Fluorescence 2007*; Geddes, C. D., Ed.; Springer: New York, 2009; Vol. *4*, pp 199−248.
(22) Callis, P. R. *Methods Enzymol.* **2011**, *487*, 1−38.
(23) Pan, C. P.; Muino, P. L.; Barkley, M. D.; Callis, P. R. *J. Phys. Chem. B* **2011**, *115*, 3245−3253.
(24) Willaert, K.; Engelborghs, Y. *Eur. Biophys. J.* **1991**, *20*, 177−182.
(25) Willaert, K.; Loewenthal, R.; Sancho, J.; Froeyen, M.; Fersht, A.; Engelborghs, Y. *Biochemistry* **1992**, *31*, 711−716.
(26) Chen, Y.; Barkley, M. D. *Biochemistry* **1998**, *37*, 9976−9982.
(27) Meech, S. R.; Lee, A.; Phillips, D. *Chem. Phys.* **1983**, *80*, 317−328.
(28) Ridley, J.; Zerner, M. *Theor. Chim. Acta* **1973**, *32*, 111−134.
(29) Cory, M. G.; Zerner, M. C.; Xu, X. C.; Schulten, K. *J. Phys. Chem. B* **1998**, *102*, 7640−7650.
(30) Liu, T. Q.; Callis, P. R.; Hesp, B. H.; de Groot, M.; Buma, W. J.; Broos, J. *J. Am. Chem. Soc.* **2005**, *127*, 4104−4113.
(31) Hager, J. W.; Demmer, D. R.; Wallace, S. C. *J. Phys. Chem.* **1987**, *91*, 1375−1382.
(32) De-Beuckeleer, K.; Volckaert, G.; Engelborghs, Y. *Proteins* **1999**, *36*, 42−53.
(33) Kubelka, J. 2011, Unpublished work.
(34) Beratan, D. N.; Betts, J. N.; Onuchic, J. N. *Science* **1991**, *252*, 1285−1288.
(35) Risser, S. M.; Beratan, D. N.; Meade, T. J. *J. Am. Chem. Soc.* **1993**, *115*, 2508−2510.
(36) Vandommelen, L.; Boens, N.; Ameloot, M.; Deschryver, F. C.; Kowalczyk, A. *J. Phys. Chem.* **1993**, *97*, 11738−11753.
(37) Ameloot, M.; Beechem, J. M.; Brand, L. *Chem. Phys. Lett.* **1986**, *129*, 211−219.
(38) Lofroth, J. E. *J. Phys. Chem.* **1986**, *90*, 1160−1168.
(39) Saladino, G.; Marenchino, M.; Gervasio, F. L. *J. Chem. Theory Comput.* **2011**, *7*, 2675−2680.
(40) Chen, J. J.; Flaugh, S. L.; Callis, P. R.; King, J. *Biochemistry* **2006**, *45*, 11552−11563.
(41) Prakash, M. K.; Marcus, R. A. *Proc. Natl. Acad. Sci. U.S.A.* **2007**, *104*, 15982−15987.
(42) Prakash, M. K.; Marcus, R. A. *J. Phys. Chem. B* **2008**, *112*, 399−404.